MRS Advances
https://doi.org/10.1557/s43580-023-00754-4

ORIGINAL PAPER

Detection of wells in images of deformed 96-wells plates

Emmanuel Rosa Delgado[1] · **José O. Sotero Esteva**[1]

Received: 28 September 2023 / Accepted: 18 December 2023

Abstract

Applications that use smartphone cameras for visual colorimetric analysis are often developed in combination with components that serve as sample holders, fluidic chambers, or active membranes. Using smartphones as handheld visual colorimetric analysis devices and sample managers with novel flexible materials raises challenges not present when using rigid materials and better-controlled settings. For instance, accurately finding where analytes are is crucial to a correct analysis. This work has used deformed 96-wells plates as a model of devices that may be used in the field in combination with smartphone applications as colorimetric devices. An algorithm based on the application of the Hough transform followed by an interpolation is developed and tested with plate images that have been deformed in a controlled fashion. The procedure accurately detects the wells in all images of the test sets.

Introduction

Visual colorimetry is a method of detecting or measuring the presence of chemical species by observing changes in color. Descriptions of such methods date back to the nineteenth century [1, 2]. Nowadays, materials science has acquired a significant role in developing nanoparticles, polymers, thin films, nanorods, nanofibers, dyes, among others, for sensor probes and in the drive towards their miniaturization [3]. The number of computer vision-based analytical procedures and systems has exponentially exploded at the beginning of the current century. More recently the use of smartphones comprises most of such reports [2, 4]. They have been used mainly in three ways: as a camera to take pictures to be analyzed later with software running on computers, as data collectors and analyzers when connected to an external device via an appropriate interface [5], and as a standalone analysis device due to the increased sophistication of their sensors. Often, these apps are developed in combination with new components that serve as sample holders, fluidic chambers, or active membranes that change colors in the presence of analytes. Some of them use novel materials that can be easily and cheaply deployed to unconventional settings outside of the lab. One example is paper-based devices for chemical assays that are designed to be analyzed with smartphone applications and data science techniques [6, 7]. They replace standard materials such as plastics and metals and sophisticated equipment, thus increasing accessibility, lowering costs, and reducing their impact on the environment.

When using smartphones as handheld visual colorimetric analysis devices and sample managers with novel materials, challenges arise that are not present in controlled settings, such as variations in illumination, position of the sample, direction, and inclination of the camera sensor that are impossible to accurately control. One example is the utilization of smartphone devices with cameras for the development of mobile applications whose aim is to analyze microwell plates assays. Detecting the specific spots of the image containing control, blank and test samples is the very first of such challenges. At the time of this writing, some apps are currently available in app-stores. For example, the *Spotxel Microplate Reader* [8] relies on presenting a template of the microwell plate superimposed on the image of the plate to be analyzed. The user must align to the physical plate shown on the phone screen. This mechanism assumes that the plate is a standard rigid plate.

In this work, the assumption of rigidity and the need to rely on the user to align the plate with a superimposed

✉ Emmanuel Rosa Delgado
emmanuel.rosa2@upr.edu

José O. Sotero Esteva
jose.sotero@upr.edu

[1] Department of Mathematics, University of Puerto Rico at Humacao, Call Box 860, Humacao 00792-0860, Puerto Rico

Published online: 04 January 2024

template have been eliminated. Removing these assumptions brings two immediate benefits: making the accuracy of measurements less dependent on the person who operates the device and allowing the option of analyzing plate images that were captured offline without the use of a specialized app. The initial steps of the algorithm, consisting of detecting the borders of the plate and correcting the keystone effect, are explained in detail. The procedure for detecting wells based on an interpolation process is also described. The efficacy of well detection is measured in a controlled manner by means of a sample of images generated by deforming the image of a rigid plate to various degrees. Its importance is that devices which hold analytes in spaces with more complex shapes would be automatically detected with modifications of the proposed method.

Materials and methods

Upon uploading or capturing an image of the microplate, the algorithm detects the plate border. The next stage involves correcting the keystone effect followed. In this section the procedure for detecting the wells is presented. Then, the Python implementation of this algorithm is discussed in detail. Finally, the procedure generating test images sets is explained.

Image preprocessing

The initial stages of this procedure are based on image preprocessing. The initial step consists of brightness equalization of the image and applying a Multidimensional Gaussian Filter [9] with the *scipy.ndimage.gaussian_filter* function, which is used to perform blurring for noise reduction. Such procedures allow for more defining edges. The edges (borders) of the microplate are located by utilizing a Sobel Filter [10] with the *filters.sobel* function. Upon finding the borders of the microplate the corners are identified as well. Perspective transformation is performed, allowing for the correction of the Keystone effect. This is accomplished with the *cv2.warpPerspective* function [11]. After this correction, the image is cropped leaving only the microplate, thus removing the inessential background.

Finding wells

Upon applying the previously mentioned image processing procedures further approaches are taken, involving blurring of the image with a Median filter. Such procedure is accomplished with the *cv2.medianBlur* function [11]. This approach is taken to reduce noise in the image, which will be beneficial for the Hough Transform algorithm. Such an algorithm is based on the detection of geometric features [12] which allows the detection of lines, circles, etc. The detection of circles with this algorithm is based on finding pixels with high gradients in light intensity using the canny algorithm [13, 14] which determines the edge points of the circles. The algorithm allows for setting constraints for the radii of the circles and their distance from each other. The wells-finding algorithm computes these constraints based on the dimensions of the size of the cropped image and the dimensions of the microplate. Upon finding the edge points of the circles in the image space (feature space) these are then used in a parameter space for the determination of parameter values of the searched shape [13]. An edge point of a circle in image space is mapped to a circle in the parameter space. Such a procedure is executed for each edge point of a circle, which gives multiple circles in the parameter space. An additional gradient constraint parameter influences the number of edge points that are considered. A lower than usual value is used to avoid spurious or overlapping circles. Consequently, in some images not all the plate's wells are going to be detected. The original color information is not altered because a copy of the original image is used in this process.

The Hough algorithm yields a set of the centers and radii of the detected wells borders. In order to find complete rows of wells a custom clustering algorithm is applied to the y-coordinates of the centers of the detected circles. Clusters which contain twelve centers of circles, complete rows, are selected. Wells in other clusters are discarded. Now, the set that is closest to the median of the y-coordinates is selected as the "reference row". An analogous process is used to select a "reference column" (Fig. 1). These two reference sets are represented as

$$R = \left\{ \left(x_j^{row}, y_j^{row}, r_j^{row} \right) : j = 1, \ldots, 12 \right\},$$
$$C = \left\{ \left(x_i^{col}, y_i^{col}, r_i^{col} \right) : i = 1, \ldots, 8 \right\}.$$

The common element of these two sets is set as the origin O. Upon establishing such a procedure, all of the well centers not in the reference axes are interpolated as

$$W_{i,j} = \left\{ w_{i,j}^k = \left(x_{i,j}^{well}, y_{i,j}^{well} \right) : i = 1, \ldots, 8, j = 1, \ldots, 12 \right\} \tag{1}$$

were

$$\begin{aligned} x_{i,j}^{well} &= d_j^x + x_j^{col}, \; d_j^x = x_j^{row} - O_x \\ y_{i,j}^{well} &= d_j^y + y_i^{row}, \; d_i^y = y_i^{col} - O_y \end{aligned} \tag{2}$$

The radii of the 96 wells are set as the average of the reference wells radii. A summary of the process is shown in Fig. 2.

Experimental

To evaluate the robustness of the algorithm, images containing the microplates were manually deformed with the *remap* function from the *OpenCV* library. The function allows the relocation of pixels in an image of N x M pixels. A cropped and keystone corrected image of a 96-wells plate is selected as a base image. The mapping process was done by mapping the pixels in the *i*th row to an inverted parabola with the mapping

$$(i,j) \rightarrow \left(i, -\frac{k}{h^2}(x-h)^2 + k\right) \tag{3}$$

where $(h,\ k)$ represents the vertex of the parabola and $h = M/2$, and k represents the number of pixels above the horizontal of the vertex. Different values of k were used in order to produce different degrees of deformation, $k = 0$, 20, 40, 60, … 200 (Fig. 3). Two sets of 10 images each corresponding to white and black colored plates were produced.

Implementation

The computer code was written in *Python* version 3.10.12. The library *Skimage* (v 0.21.0) [10] was used for image I/O, color mode conversions, filtering pixels (*threshold_minimum, sobel*, *scharr*), *Numpy* (v 1.25.2) [15] for numerical and arrays computations, *Scipy* (v 1.11.2) [9] were used for *gaussian_filter*, *linregress*, from *OpenCV* (v 4.7.0) [11] perspective transformations related to keystone correction and *opencv. remap* for image bending were used. Graphical outputs were produced with *Matplotlib* (v 3.7.2) [16].

Results

The utilization of the Hough algorithm demonstrated its capability of detecting well's centers (circles). However, the algorithm is very sensitive to its *accumulator threshold* parameter. For lower values, it tends not to find all 96 wells while for higher values it detects either many spurious circles (for example, circles completely outside wells) or many circles for some wells. Getting it to consistently detect exactly 96 wells was not possible for a diversity of images. Thus, the necessity of using lower values for the parameter which consistently underestimated the wells detected but gave some complete rows and columns of wells (Fig. 1a) and to find the missing ones by interpolation. With the implementation of interpolation for those missing centers of the wells, the robustness of the algorithm improved drastically, as shown in Fig. 1b.

Figure 3 presents a sample of plates with different degrees of deformation and the wells detected by the implemented algorithm. The pictures were taken in a common room environment with fluorescent light illumination.

To quantify the precision of the wells' positions we define the error sets

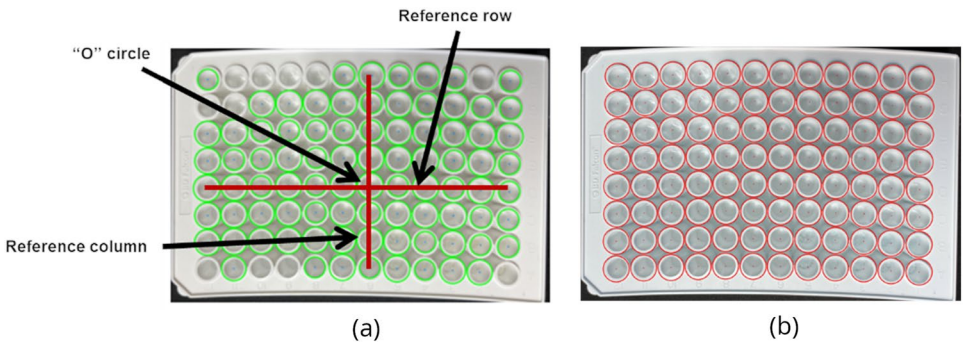

Fig. 1 Finding wells using interpolation. **a** wells found by Hough algorithm are marked in green, reference row and column are chosen as well as the origin. **b** wells computed by formulae (2) above

Function *extrapolated_wells(image):*
Input*: image as N × M×C array*
Output*: list of triples (x coordinate, y coordinate, radius)*

Copy, grayscale, and blur the original image
Detect edge-pixels using the Canny algorithm
Detect circles that are candidates to be wells edges using Hough Transform
Remove outlier circles
Find rows of 12 circles
Find columns of 8 circles
Choose a row and a column closest to the center of the image as references
Set Origin as common circle in reference row and column
Interpolate the rest of the wells using the origin and reference row and column

Fig. 2 Plate Wells detection algorithm

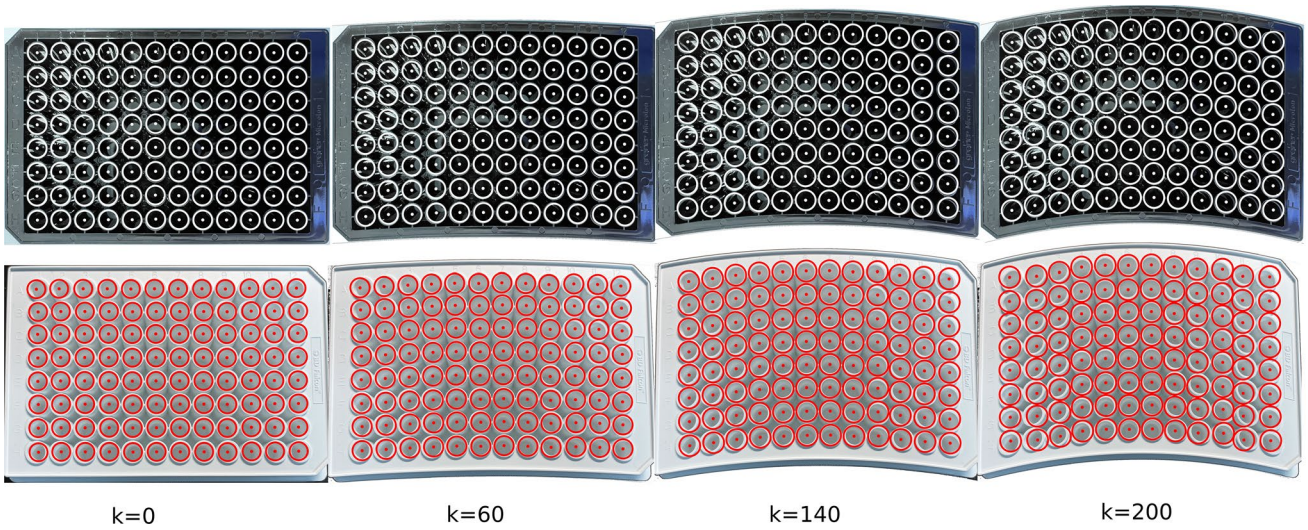

Fig. 3 Plates with different amounts of deformations starting from undeformed plates ($k=0$) to maximum deformation ($k=200$) for black and white plates. Wells detected with the implemented algorithms are shown as white or red circles, respectively

$$E(k) = \left\{ d\left(c_{i,j}^{k}, w_{i,j}^{k}\right), i = 1, \cdots, 8, j = 1, \cdots, 12 \right\}$$

where k is the deformation parameter defined above $c_{i,j}^{k}$ is the *actual* center of the well in row i, column j in the plate deformed by k pixels, $d\left(c_{i,j}^{k}, w_{i,j}^{k}\right)$ is the distance between $c_{i,j}^{k}$ and the detected center $w_{i,j}^{k}$ as defined in Eq. (1). The coordinates of the actual centers $c_{i,j}^{0}$ of the undeformed plate with $k=0$ were obtained by visually identifying the center of the four corner wells and computing the rest of the centers of the undeformed plate by interpolation according to Eq. (2). To compute $c_{i,j}^{k}$ for $k>0$ the deformation formula (3) was applied to the centers $c_{i,j}^{0}$.

Figure 4 shows the behavior of the sets $E(k)$, the difference between detected wells centers and exact centers, for the white and black plates. As expected, average errors tend to increase as deformation increases. The black plate produced smaller errors than white's. The violin's plot also shows that the distribution of the errors for each plate tend to be skewed with most errors tending to fall below the average with a few large errors when compared to averages.

The maximum average error was 19.37 pixels for white plates and 12.92 pixels for black plates. The average error across all plates was 12.74 pixels. Given that the cropped images are larger than 2000 by 3000 pixels, this average error represents less than 0.35% of the diagonal of the plate's image. Considering that the diameters of the wells in Fig. 3 are about 170 pixels, the average error would be less than 10% of the well diameter. Considering the information inferred from the violin plots these errors are lower for most wells.

Figure 4 (insert) represents the average errors per well. For each plate well, average distances between detected and expected well centers were considered across all sample plates at the same position. Detected centers tend to be less accurate for corner wells. Since the proposed algorithm prioritizes reference axes' origins closer to the center of the plate, corner wells correspond to the wells farthest from the origin. This is consistent with the expected behavior from an interpolation process.

The algorithm was tested under the additional illumination sources found in the literature when evaluating the accuracy of colorimetric methods using smartphones [18–21]. Plates were illuminated with camera flash, LED, indirect sunlight and ultraviolet. Qualitatively the results were like the ones described above. The table 1 shows that the

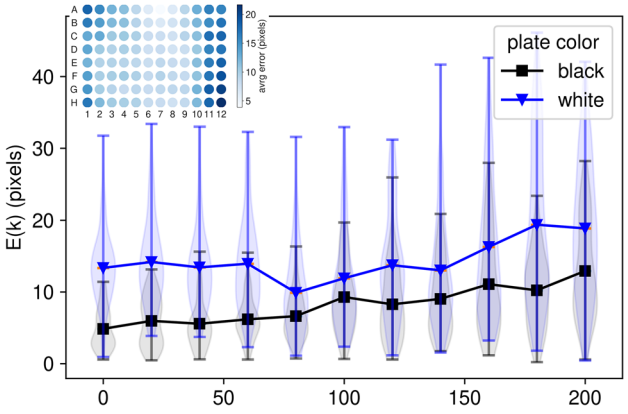

Fig. 4 Analysis of errors in wells' localizations. Violin plot of the errors in wells center's locations for various levels of deformations k. Average errors per deformation are joined by lines. Insert: heatmap representing error averages per plate well in all samples

Table 1 Average errors in well location for all deformations among the different plates and illumination sources

Illumination type	Average error	
	White plates	Black plates
Fluorescent	19.37	12.92
LED lamp	8.56	24.35
Camera flash	13.53	17.17
Indirect sunlight	17.09	16.42
Ultraviolet lamp	11.82	n/a

variations of the average errors for both types of plates are similar among all illumination sources.

Discussion

This work has used deformed 96-well plates as a model of devices that may be used out of laboratories in combination with smartphone applications as colorimetric devices. Although the Hough transform alone is not robust enough to find the edges of exactly the 96 wells of the deformed plates under varying conditions, the implementation of the interpolation presented here improves the robustness of the algorithm. Further applications to other types of devices are plausible, such as for the detection of moving targets. Furthermore, the original Hough transform was formulated to detect straight segments in images. Thus, by using a similar interpolation method, polygonal features of the devices holding analytes may be detected. Moreover, with further modifications of the base Hough method [22], other more complex shapes present in devices such as mixers, separators, and other fluidic devices would be automatically detected.

The algorithm's main limitation is in the detection of the edges of the microplate during the image preprocessing stage. This is due to factors such as shadows, specular light reflections on shiny backgrounds, and background patterns that produce spurious edge detections. These factors prevent the algorithm from achieving plate detection and an efficient correction of the keystone effect. However, once the microplate is successfully located, the proposed method shows robustness in detecting the wells (circles) in the plate. An appropriate accumulator threshold parameter of the Hough transform algorithm can be automatically found for the given picture. Further challenges may involve smartphones cameras that often process the images in unspecified ways to enhance the visual appeal of the pictures. However, these aspects pertain more to colorimetric analysis of the wells' contents which are out of the scope of this work.

Works in literature specifically dealing with 96-wells microplate readers using smartphones such as the *Spotxel Microplate Reader* [8] rely on presenting a template of the microwell plate superimposed on the image of the plate to be analyzed and do not attempt to automatically detect the wells. Y. Chen et.al. [23] use a convolutional neural network to detect the content of a smaller 8×8 microwell plate. They use a correlation between the network classification and the training set as an accuracy measurement that is not directly related to well detection. G.C. Ravichandran [24] uses the Hough transform to detect microwells in a device with 10195 wells. He does not report the accuracy as it is done here but does report an accuracy between 99.4% and 100% of well detection, noting some difficulties in detection of wells close to corners which the present algorithm detects by interpolation. C. Militello *et. al* [25]. also uses the Hough transform on relatively flat cell-culture plates with a varying number of wells (6–48 wells). They consider detection of wells in inclined plate positions but not deformed plates. As in the present work adjustments to the accumulator threshold parameter are performed but they rely on detecting overlapping circles and selecting the first n wells according to a circle strength value. Accuracy of the method is measured based on a comparison between cell-cultures detected manually and by their method. No accuracy of the location of the wells is reported.

Acknowledgments The authors acknowledge the help of Dr. Vibha Bansal and Dr. Ezio Fasoli's groups from the Departments of Chemistry of the University of Puerto Rico at Cayey and Humacao campuses respectively who provided materials and test images for this work. They also thank the anonymous reviewer who suggested testing with different illumination sources as it better demonstrates the robustness of the method. This work is sponsored by the PENN-UPR *Partnerships for Education and Research in Materials* program (NSF-DMR-2122102).

Author contributions ER-D: Investigation, methodology, and writing—original draft. JOSE: Funding acquisition, project administration, resources, and supervision. Both authors contributed equally in: conceptualization, data curation, software, validation, visualization, formal analysis, and writing—review and editing.

Funding This material is based upon work supported by the *PENN-UPR Partnerships for Education and Research in Materials* program, which is supported by the National Science Foundation under Grant NSF-DMR-2122102.

Data availability The computer code and the test images that reproduce all the results of this work are available at the *Open Science Framework* platform, component *Deformed plate wells finder* at https://osf.io/7yvf3/?view_only=a1be11da5df149a9ad1d290618afd63b [17].

Declarations

Conflict of interest The authors declare no conflict of interest.

References

1. F. Szabadváry, A. Robinson, *Comprehensive Analytical Chemistry* (Elsevier, Amsterdam, 1980). https://doi.org/10.1016/B978-0-444-41859-3.50008-6
2. G.M. Fernandes, W.R. Silva, D.N. Barreto, R.S. Lamarca, C.F. Paulo, L. Gomes, J. Flávio, S. da Petruci, A.D. Batista, Anal. Chim. Acta **1135**, 187–203 (2020). https://doi.org/10.1016/j.aca.2020.07.030
3. V.S. Ajay Piriya, P. Joseph, S.C.G. Kiruba Daniel, S. Lakshmanan, T. Kinoshita, S. Muthusamy, Mater. Sci. Eng. C **78**, 1231–1245 (2017). https://doi.org/10.1016/j.msec.2017.05.018
4. L.F. Capitán-Vallvey, N. Lopez-Ruiz, A. Martinez-Olmos, M.M. Erenas, A.J. Palma, Anal. Chim. Acta **899**, 23–56 (2015). https://doi.org/10.1016/j.aca.2015.10.009
5. S. Banik, S.K. Melanthota, Arbaaz et al., Anal. Bioanal. Chem. **413**, 2389–2406 (2021). https://doi.org/10.1007/s00216-021-03184-z
6. Y. Fan, J. Li, Y. Guo, L. Xie, G. Zhang, Measurement **171**, 108829 (2021). https://doi.org/10.1016/j.measurement.2020.108829
7. B.R. Sun, A.G. Zhou, X. Li, H.Z. Yu, ACS Sens. **6**(5), 1731–1744 (2021). https://doi.org/10.1021/acssensors.1c00512
8. N. Qin, Z. Liu, L. Zhao et al., Anal. Sci. **39**, 139–148 (2023). https://doi.org/10.1007/s44211-022-00216-1
9. P. Virtanen, R. Gommers, T.E. Oliphant et al., Nat. Methods **17**, 261–272 (2020). https://doi.org/10.1038/s41592-019-0686-2
10. S. van der Walt, J.L. Schönberger, J. Nunez-Iglesias, P. Boulogne, J.D. Warner, N. Yager, E. Gouillart, T. Yu, the scikit-image contributors, PeerJ **2**, e453 (2014). https://doi.org/10.7717/peerj.453
11. G. Bradski, Dr. Dobb's J.: Softw. Tools Prof. Program. **25**(11), 120–123 (2000)
12. P.E. Hart, IEEE Signal Process. Mag. **26**(6), 18–22 (2009). https://doi.org/10.1109/MSP.2009.934181
13. H. Yuen, J. Prinsen, J. Illingworth, J. Kittler, Image Vision Comput. **8**(1), 71–77 (1990). https://doi.org/10.1016/0262-8856(90)90059-e
14. J. Canny, IEEE Trans. Pattern Anal. Mach. Intell. **6**, 679–698 (1986). https://doi.org/10.1109/TPAMI.1986.4767851
15. C.R. Harris, K.J. Millman, S.J. van der Walt et al., Nature **585**, 357–362 (2020). https://doi.org/10.1038/s41586-020-2649-2
16. J.D. Hunter, Comput. Sci. Eng. **9**(03), 90–95 (2007). https://doi.org/10.1109/MCSE.2007.55
17. J.O. Sotero Esteva, and E.R. Delgado, Detection of Wells in Images of Deformed 96-Wells Plates. (OSF, 2023). https://osf.io/7yvf3/?view_only=a1be11da5df149a9ad1d290618afd63b. Accessed 26 September 2023.
18. M. Nixon, F. Outlaw, T.S. Leung, PLoS ONE **15**(3), e0230561 (2020). https://doi.org/10.1371/journal.pone.0230561
19. V. Doğan, E. Yüzer, V. Kılıç, M. Şen, Analyst **146**(23), 7336–7344 (2021). https://doi.org/10.1039/D1AN01888D
20. A.Y. Mutlu, V. Kılıç, G.K. Özdemir, A. Bayram, N. Horzum, M.E. Solmaz, Analyst **142**(13), 2434–2441 (2017). https://doi.org/10.1039/C7AN00741H
21. M. Ra, M.S. Muhammad, C. Lim, S. Han, C. Jung, W.-Y. Kim, IEEE J. Transl. Eng. Health Med. **6**, 1–11 (2018). https://doi.org/10.1109/JTEHM.2017.2765631
22. M.C. Beltrametti, A.M. Massone, M. Piana, SIAM J. Imaging Sci. **6**(1), 391–412 (2013). https://doi.org/10.1137/120863794
23. Y.C. Chen, Z. Zhang, E. Yoon, Anal. Chem. **92**(11), 7717–7724 (2020). https://doi.org/10.1021/acs.analchem.0c00710
24. G. C. Ravichandran (2020). University of Kansas ProQuest Dissertations Publishing, 2020. 28000563.
25. C. Militello, L. Rundo, V. Conti, L. Minafra, F.P. Cammarata, G. Mauri, M.C. Gilard, N. Porcino, Comput. Biol. Med. **89**, 454–465 (2017). https://doi.org/10.1016/j.compbiomed.2017.08.005